

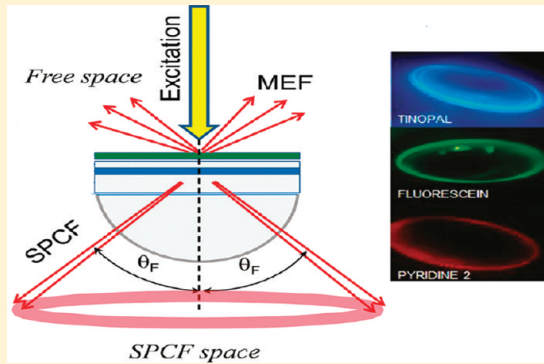
UV to NIR Surface Plasmon Coupled and Metal-Enhanced Fluorescence Using Indium Thin Films: Application to Intrinsic (Label-less) Protein Fluorescence Detection

Hirdyesh Mishra,[†] Anatoliy Dragan,[†] and Chris D. Geddes^{*†,‡}

[†]The Institute of Fluorescence and [‡]Department of Chemistry & Biochemistry, University of Maryland Baltimore County, 701 East Pratt Street, Baltimore, Maryland 21202, United States

 Supporting Information

ABSTRACT: Surface plasmon coupled fluorescence (SPCF) and metal enhanced fluorescence (MEF) over a broad wavelength range from UV to NIR are demonstrated from 20 nm thin indium films. Steady-state and time-resolved fluorescence measurements of fluorophores deposited on the indium thin films indicate enhancement of the fluorescence intensity along with decreases in decay times, both in MEF and SPCF modes, accompanied by an increase in photostability. MEF was found to be more pronounced for the red emission dye with respect to a blue emission dye. A completely *p*-polarized directional emission for three fluorophores from a hemicylindrical prism at 44° indicates surface plasmons couple with the near field dipoles at the interface of the indium-sample. The evanescent waves generated at the interface are calculated to penetrate more deeply for longer wavelength excitation with respect to shorter wavelengths, and the penetration depth nearly doubles in comparison to that of the widely used silver thin films. As an application, indium thin films have been used for intrinsic protein chromophore (tryptophan) fluorescence detection. Nearly a 3.5-fold enhancement of intrinsic protein fluorescence along with a decreased decay time and increase in photostability were observed with SPCF. Subsequently, indium thin films can be utilized as a single assay platform in surface plasmon fluorescence spectroscopy (SPFS) over a broad spectral range and can potentially be a much better choice than other metallic thin films.



1.0. INTRODUCTION

Recently, the surface plasmon coupled fluorescence (SPCF) phenomenon has become a rapidly progressive area of research in the field of analytical biosciences to understand biomolecular kinetics and binding events at interfaces.^{1–10} SPCF spectroscopy is a more sensitive analytical tool with respect to the closely related surface plasmons resonance (SPR) technology.^{11–13} Surface plasmons are coherent collective oscillating electrical charges between a metal–dielectric interface. When a thin metal film is illuminated by radiation in a suitable angle through a prism, the surface plasmons start to resonate with an incident photon frequency, thereby reducing the reflected light intensity at that particular angle by absorbing resonant photons. The SPR angle is sensitive to the refractive index of the sample above the metal, distal from the glass prism. The origin of this sensitivity is the evanescent field from the plasmons, which penetrates several nanometers into the sample. However, binding events for a very low concentration of analyte typically cannot produce enough change in the SPR angle and so conversely, the SPR technique is hinged on the ability to detect very small changes in angle. This sensitivity limitation with the SPR technique can be overcome by detecting fluorescence excited by the evanescent field associated with surface plasmons. There are various reports on the utilization

of SPCF in bioassays.¹⁴ These include studies for DNA hybridization,^{15,16} immunoassays,¹⁷ ultrafast assays,^{18,19} and protein detection,²⁰ etc. In all of these reports, one of the biological assay components is linked or positioned close to the metal surface, and their interactions with the biomolecule of interest in the presence of a third fluorophore-labeled biomolecule is monitored via the change in SPCF intensity from the back of the prism. Subsequently, the concentration of the biomolecule of interest is directly calculated from the SPCF intensity.

In surface plasmon fluorescence spectroscopy (SPFS), the excitation of the fluorophores can be achieved directly from the sample side (reverse Kretschmann (RK) configuration) or through a prism side (Kretschmann (KR) configuration). In the RK configuration,²¹ fluorophores are directly excited by the incident excitation source, and the resulting fluorescence emission induces and couples to surface plasmons. In the KR configuration, the excitation light entering through the prism generates the surface plasmons in the metal film and excites fluorophores within a certain distance (typically 10 to 200 nm) from the surface. Below

Received: July 18, 2010

Revised: July 27, 2011

Published: July 28, 2011

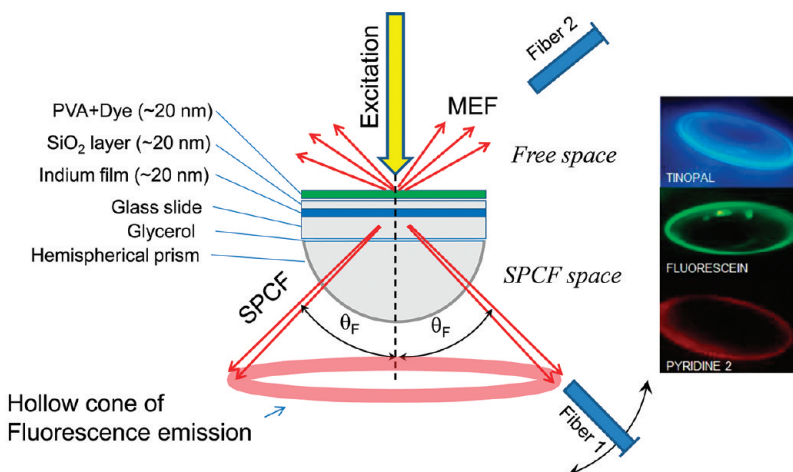


Figure 1. (Right) Schematic representation of the reverse Kretschmann (RK) experimental setup for surface plasmon coupled fluorescence (SPCF) measurements. A hemispherical prism was used to collect SPCF emission in “SPCF space” by using an optical fiber (Fiber 1) for the different dyes loaded on metallic films. MEF in the free space was collected using an optical fiber (Fiber 2), and spectra were measured by the compact Ocean optics photometer. (Left) Real color photographs of the SPCF emission “rings” taken for the tinopal, fluorescein, and pyridine PVA films. Θ_F is an angle of directional SPCF emission, which forms a hollow cone in space relative to the sample surface normal.

10 nm, fluorescence typically decays through nonradiative channels, often referred to as fluorescence damping or quenching.^{22,23} In the case of the reverse Kretschmann (RK) configuration, the fluorescence emission can be detected from the sample side (free space fluorescence) and/or from the back of the metal film (SPCF space) (see the experimental setup in Figure 1). The free space emission is isotropic, while SPCF emission is highly directional; it propagates in a hollow cone with a cone angle, Θ_F (Figure 1). Despite the fact that the spectral properties of the SPCF radiation are essentially identical to those of the fluorophore emission in free space, emission of SPCF is highly *p*-polarized,³⁵ i.e., anisotropic. The cone (Θ_F) angle of SPCF emission propagation coincides with the angle of metal’s minimum reflectivity and varies with the type of metal used, subsequent over layers present on the metallic films, and the wavelength of the excitation source. The SPCF angle is narrow, especially for metals with a low ϵ_i/ϵ_r ratio. Subsequently, in applications based on these metal films, the detection optics must be adjusted for the varying observation angle, which can significantly decrease the experimental error in the collection of data. In this regard, the data collection efficiency of the SPCF technique can be significantly improved by fixing the observation angle, similar to that of a traditional fluorescence spectrometer. Both configurations are highly attractive in analytical sensing applications.^{24,25}

Recently, Geddes²⁶ reviewed the surface plasmon coupled luminescence (SPCL) of 11 different metals having different optical and electrical properties in different spectral regions. They developed a most useful flowchart model on the basis of Fresnel computational calculations for selection of metal, wavelength, and angle for a variety of desired SPCL-based applications. To date, zinc²⁷ and aluminum²⁸ thin films have been used in the UV spectral range, while silver,²⁹ nickel,³⁰ and zinc³¹ thin films have been used in the visible spectral range; nickel,³¹ gold,³² and copper³³ thin films were also shown to work in the red spectral region. Iron thin films can also be used for a fixed angle measurement of visible radiation.³⁴

In this work, the applicability of indium thin films is demonstrated both theoretically and experimentally. Theoretical Fresnel calculations were employed to determine the optimum

thickness for the generation of surface plasmon modes in indium thin films. Fresnel calculations were also used in the investigation of the spectral range where the surface plasmons in indium can effectively be generated as well as in direct comparison with other metal films.²⁷ In this regard, to demonstrate the applicability of indium thin films for use in SPFS, 20 nm indium thin films with a 20 nm SiO_x overlayer were thermally evaporated onto glass/quartz supports that have optical transmission above 320 nm. Surface plasmon coupled and free space fluorescence from fluorophores with emission in the ultraviolet and visible spectral regions were measured using the reverse Kretschmann configuration. The theoretical calculations and experimental data are in very good agreement. Finally, we place our findings in context with the detection of intrinsic protein fluorescence, i.e., label-less detection, where the penetration depth into optically dense media can be both modeled and tuned using different metallic thin film sensing supports.

Recently, we have shown that indium nanoparticles demonstrate the pronounced MEF effect for chromophore (tryptophan and tyrosine chromophores, and whole protein (BSA)) solutions in the UV spectral region.³⁶ In this study, we investigate indium film optical properties, i.e., the ability to show SPCF and enhance chromophore fluorescence in dry films, in the broad spectral region.

2.0. EXPERIMENTAL SECTION

2.1. Materials. All fluorophores, tinopal-CBS, sodium fluorescein, *N*-acetyl-tryptophan-amide (NATA), pyridine-2, poly(vinyl) alcohol (PVA, 98% hydrolyzed 13,000–23,000 MW), and silane-prep glass microscope slides were purchased from Sigma-Aldrich Chemical Co. (Milwaukee, WI, U.S.A.). Indium wire (99.99%) was purchased from Kurt J. Lesker, USA. Quartz (75 mm × 25 mm) slides were purchased from Ted Pella Inc. CA, USA.

2.2. Methods: Sample Preparation. A 20 nm thin layer of indium was deposited on both quartz and glass slides followed by a 20 nm SiO_x protective layer using an Auto 306 Vacuum coater (Accu Coat Inc., Rochester, NY, USA). The thicknesses of the

Table 1. Intensity Decay Parameters of Red, Green, and Blue Dyes Doped in PVA and Coated on 20 nm Indium + 20 nm SiO₂ ($\lambda_{\text{ex}} = 445 \text{ nm}$)^a

fluorophores	sample	τ_1 (ns)	τ_2 (ns)	τ_3 (ns)	α_1	α_2	α_3	$\langle \tau \rangle$	$\bar{\tau}$	χ^2
pyridine-2 (red) E.F. = 7.5	glass slide	0.99	0.14	2.39	42	15	43	1.97	1.46	1.137
	free space	0.93	0.10	2.30	50	14	36	1.78	1.31	1.342
	SPCF space	0.87	0.16	1.80	37	28	33	1.41	0.96	1.241
sodium fluorescein (green) E.F. = 5.2	glass slide	4.18	0.15		98	2		4.19	4.09	1.041
	free space	3.88	0.24	1.82	22	10	68	2.63	2.11	1.417
	SPCF space	3.28	0.17	1.57	27	25	48	2.43	1.68	1.372
tinnnni-CRS (blue) E.F. = 3.5	glass slide	1.20			100			1.20	1.20	1.211
	free space	1.18	0.15		40	60		0.56	1.02	1.217
	SPCF space	1.15	0.11		30	70		0.42	0.96	1.189

^a SPCF = surface plasmon coupled fluorescence. E.F. = free space enhancement factor. $\langle \tau \rangle$ = amplitude weighted decay time. $\bar{\tau}$ = mean decay time.

deposited film was monitored by a quartz crystal microbalance. Fluorophores were deposited onto the indium thin films by spin coating a solution of polymers containing the fluorophore. Stock solutions of 1 μM tinopal-CBS, 1 μM sodium fluorescein, and 1 μM pyridine-2 were prepared in water and mixed in 0.1% (w/v) of PVA. The final concentrations of the fluorophore/polymer solutions were adjusted to 0.1 μM . Forty microliters of fluorophore/polymer solution was spin-coated onto SiO_x thin films (1 cm × 1 cm) using a Chemat Technology Spin Coater (Model KW- 4A) with the following speeds: 3000 rpm setting 1, 9 s; setting 2, 30 s. The thickness of the polymer films was previously measured to be \approx 20 nm for 0.1% (w/v) PVA films.²⁷ The reference slide, for the control experiment, was prepared from identical 0.1% (w/v) PVA solution but without fluorophores.

2.3. Surface Plasmon Coupled Fluorescence (SPCF) Measurements. For free space and SPCF space measurements, the spin-coated slides of indium were attached to a hemicylindrical quartz prism using a nonfluorescent index matching fluid (mixture of propylene glycol $n \approx 1.43$ and acetophenone $n \approx 1.53$). This combined sample was positioned on a precise rotary stage ($x-z$) that allows excitation and observation at any desired angle relative to the vertical axis (z -axis) around the hemicylindrical prism. The sample was excited using the reverse Kretschmann configuration from the air or sample side, which has a refractive index lower than that of the prism. The excitation of tinopal and sodium fluorescein was undertaken with a 405 nm laser line, while pyridine-2 was excited using a 473 nm laser at an angle of 90°. A schematic representation of the experimental setup for surface plasmon coupled fluorescence (SPCF) measurements is shown in Figure 1. A hemispherical prism was used to collect the “rings” of emission for the different dyes from the films. The observation of the surface plasmon coupled fluorescence and free space emission was performed with a 600 μm diameter fiber bundle, covered with a 200 μm vertical slit, positioned about 15 cm from the sample. This corresponds to an acceptance angle below 0.1°. The output of the fiber was connected to an Ocean Optics HD2000+ spectrofluorometer in order to measure the fluorescence emission spectra of the different fluorophores. SPCF from four fluorophores emitting in different wavelength ranges were measured using a hemispherical prism and a commercially available spectrofluorometer (Ocean Optics, Inc., Florida, USA). Real-color photographs of the SPCF rings are shown in Figure 1, taken through an emission filter with a Canon Power shot S50 Digital Camera.

2.4. Instrumentation. Absorption spectra of sample films were collected using a single beam Varian Cary 50-Bio UV-vis

spectrophotometer. Emission spectra were collected using a Varian Cary Eclipse fluorescence spectrophotometer using a pulsed xenon source for excitation. A front face sample geometry was used to undertake all the fluorescence measurements with the spectral slit width of 5 nm, in both the excitation monochromator and the emission monochromator channels. Fluorescence decays were measured using a Horiba Jobin Yvon Tem-Pro fluorescence lifetime system using the time-correlated single photon counting (TCSPC) technique with a TBX picosecond detection module. The excitation source was a pulsed LED source (from IBH) of wavelength 372 nm, having a maximum repetition rate of 1.0 MHz and a pulse duration of \approx 1.1 ns. The intensity decays were analyzed by decay analysis software (DAS) version 6.4, in terms of the multiexponential model:

$$I(t) = \sum_i \alpha_i \exp(-t/\tau_i) \quad (1)$$

where α_i is the amplitude, and τ_i is the decay time; $\sum_i \alpha_i = 1.0$. The fractional contribution of each component to the steady-state intensity is given by

$$f_i = \frac{\alpha_i \tau_i}{\sum_j \alpha_j \tau_j} \quad (2)$$

The mean lifetime of the excited state is given by

$$\bar{\tau} = \sum_i f_i \tau_i \quad (3)$$

and the amplitude-weighted lifetime is given by

$$\langle \tau \rangle = \sum_i \alpha_i \tau_i \quad (4)$$

The values of α_i and τ_i were determined by nonlinear least-squares impulse deconvolution analysis with the goodness of the fit judged by the residuals, autocorrelation function, and χ^2 values (Table 1). The measurement error in decay time is of the order of 0.01 in the nanosecond range. Photostability experiments (steady-state intensity decay) were undertaken using a 405 nm laser coupled with a neutral density filter and Ocean Optics Spectrophotometer HP2000, where the fluorescence intensity was measured as a function of time.

2.5. Theory and Fresnel Calculations. The theory of SPCF is analogous to SPR.⁷ In SPCF, when a metal film is radiated by both free space and prism space, the near field excitation of fluorophores is coupled with the creation of surface plasmons at the metal–prism interface. Therefore in SPCF, the angular distribution of radiated light can be determined by the same

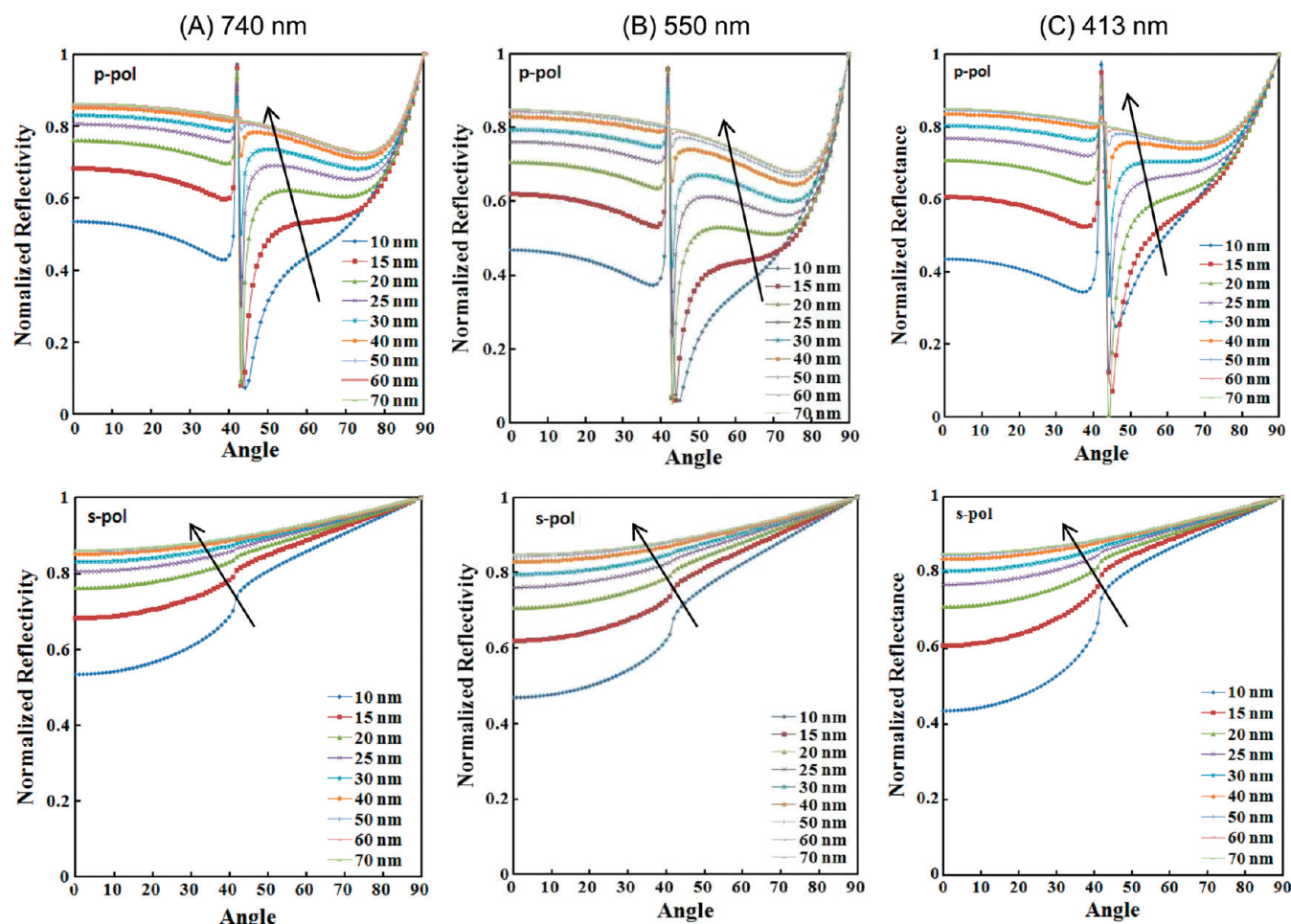


Figure 2. Three-phase Fresnel reflectivity curves for *p*-(top) and *s*-(bottom) polarized light at (A) 740 nm, (B) 550 nm, and (C) 413 nm for indium substrates ranging from 10 to 70 nm deposited on glass plates.

wave-vector matching condition as in SPR. Since *s*-polarized light propagating along the *x*-direction possess only an electric field parallel to the surface (*y*-direction), it can be effectively canceled out by its mirror image on the surface. Subsequently, *p*-polarized light that has an electromagnetic component normal to the surface can most efficiently generate surface plasmons. The *p*-polarized light source also generates an evanescent electromagnetic wave across the metallic sample interface, along the *x*-axis. Surface plasmons are excited, and couple fluorophore quanta only at a specific angle (θ_{SP}), where reflectivity is a minimum value for wave vector matching at the sample–metal interface. This wave vector matching condition is given as

$$k_{SP} = k_0 n_p \sin \theta_{SP} \quad (5)$$

where k_0 is a wave vector of incident light in air, n_p is the reflective index of prism, and θ_{SP} is the surface plasmon angle. Coupling of the fluorescence with the metal surface depends on the matching of the wave vector of incident light (k_0) with the wave vector of surface plasmons by the following equation:

$$k_{SP} = k_0 \sqrt{\frac{\epsilon_m \epsilon_s}{\epsilon_m + \epsilon_s}} \quad (6)$$

where ϵ_m and ϵ_s are the real part of the dielectric constant of the metal and the sample, respectively. At θ_{SP} , the metal surface acts

as a resonator for incident light and gives rise to the resonant excitation of a surface plasmon, which reradiates according to the dispersion curve for surface plasmons. Fresnel calculations were undertaken by using a macro-procedure written for Igor Pro software. In these calculations, surface plasmon resonance conditions were performed to the different optical properties of each dielectric layer and their respective thicknesses. A typical result of these calculations is the so-called reflectivity curves. The reflectivity curves are a result of surface plasmon excitation by light and typically have a narrow “dip” at a certain angle with a minimum value reaching close to zero in the most ideal situation. The half-width of the reflectivity curve for metals is different, mostly due to their differences in the value of the imaginary part of their dielectric function. The extent of shift in the angle of minimum reflectivity predominantly depends on the thickness of the additional dielectric layers. These plasmons then radiate into the glass substrate at the surface plasmon angle for the emission wavelength. The plasmons radiate at the plasmon angle because this is needed to wave vector match, i.e., conservation of the angular momentum. The plasmons cannot radiate into the sample because the wave vector cannot be matched. The angle θ_{SP} depends on the wavelength, as k_x (the wave vector in the *x*-direction) and the optical properties of the metal depend on the wavelength. Free space (FS) emission of the fluorophores can

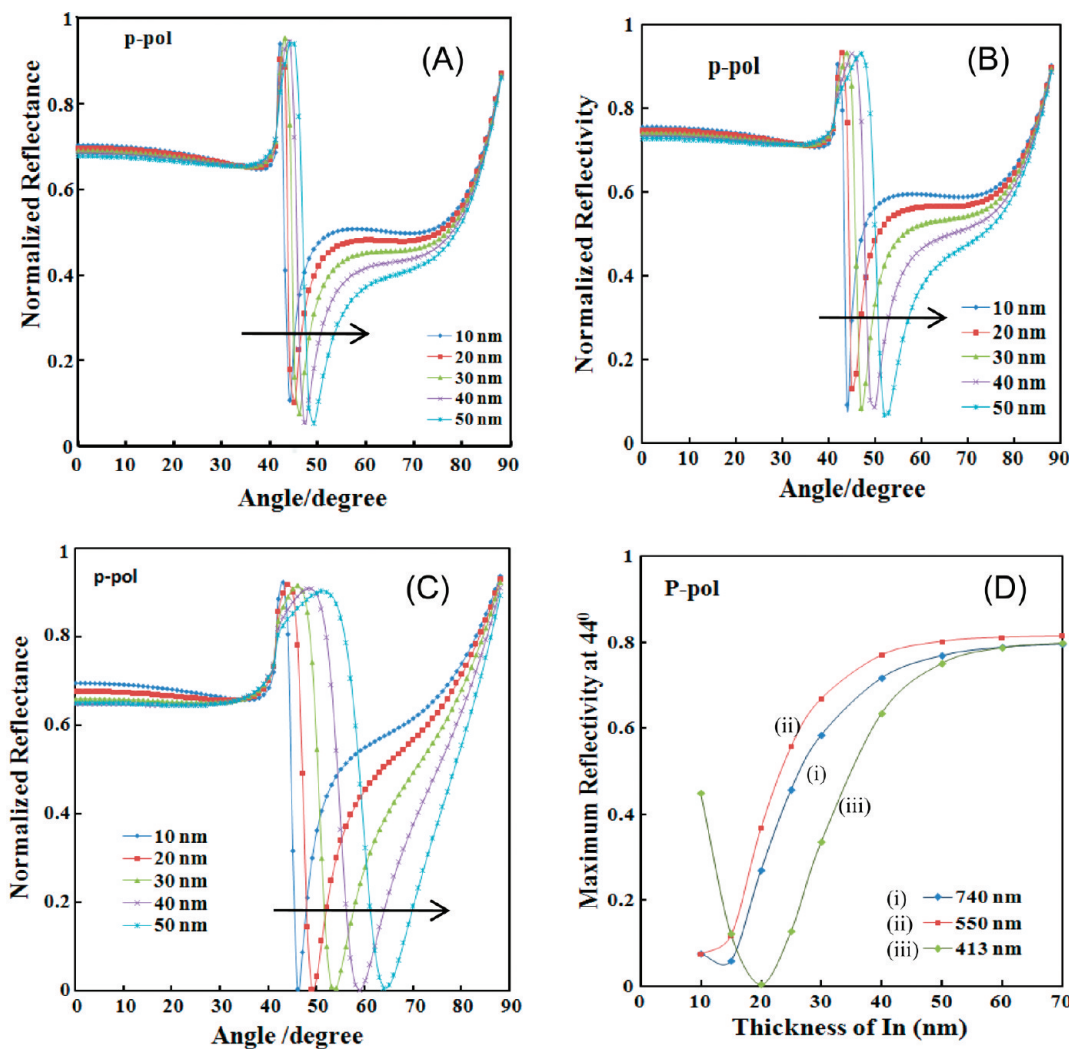


Figure 3. Four-phase Fresnel reflectivity curves for *p*-polarized light at (A) 740 nm, (B) 550 nm, and (C) 413 nm for indium substrates (20 nm) with SiO_2 thicknesses ranging from 10 to 50 nm coated onto glass plates. (D) Fresnel maximum reflectivity curves at 44° for *p*-polarized light at three different wavelengths for SiO_2 thicknesses ranging from 10 to 50 nm coated on indium deposited (20 nm) glass plates.

also occur for dipoles not *p*-oriented or for dipoles distal from the surface.

Because of the complex nature of ϵ_m and k_x , surface plasmon modes propagate along the metal/sample interface at a finite length (penetration length), dependent on the imaginary component of the wave vector, k_x . In addition, the evanescent wave has a maximum amplitude at the interface ($Z = 0$) and decays exponentially into the sample and the metal. The penetration depth of this light into the dielectric medium is calculated to be a few hundred nanometers.¹⁰ Three-phase (glass/metal/air) Fresnel calculations were also undertaken for penetration depth studies for indium thin films. The maximum value for the *z*-component of the electric field that occurs at the angle of reflectivity minimum is normalized with respect to the highest value and plotted against the thickness (depth) above the metal.¹² The real and imaginary parts of the dielectric constant for different wavelengths were obtained from Lumerical Finite Difference Time Domain (FDTD) Solution software (Vancouver, Canada) and the corresponding reflective index, n , and extinction coefficient (imaginary part of the complex index of refraction), k , were

calculated by the relationship, $\epsilon_1 = n^2 - k^2$ and $\epsilon_2 = 2nk$, respectively (see Table 1 in the Supporting Information).

The dependence of SPR upon the refractive index of the sample is due to the evanescent field from the plasmons, which penetrate into the sample and decay exponentially away from the metal surface.¹⁴ On the basis of the analogy between SPR and SPCF, we expect that fluorophore coupling to the metal also depends on the depth of the evanescent field. For SPR, the electrical field decays exponentially as $E_{\text{sp}}(Z) = E_0 \exp(-k_z Z)$ (where E_0 is the field strength at $Z = 0$), and $k_z^{-1} = [k_{\text{SP}}^2 - \epsilon_s(\omega/c)^2]^{0.5}$ is the penetration depth of the evanescent field into the sample, where ω is the frequency of the incident light.

3.0. RESULTS AND DISCUSSION

Since Fresnel calculations predict the interactions of light with metal thin films, they are an important tool for the design of metal surfaces for SPCF applications. Three phase (glass/metal/air) Fresnel reflectivity computational calculations for different angles of *p*-polarized and *s*-polarized light at wavelengths 740, 550, and 413 nm for indium thin films of thickness ranging from 10 to

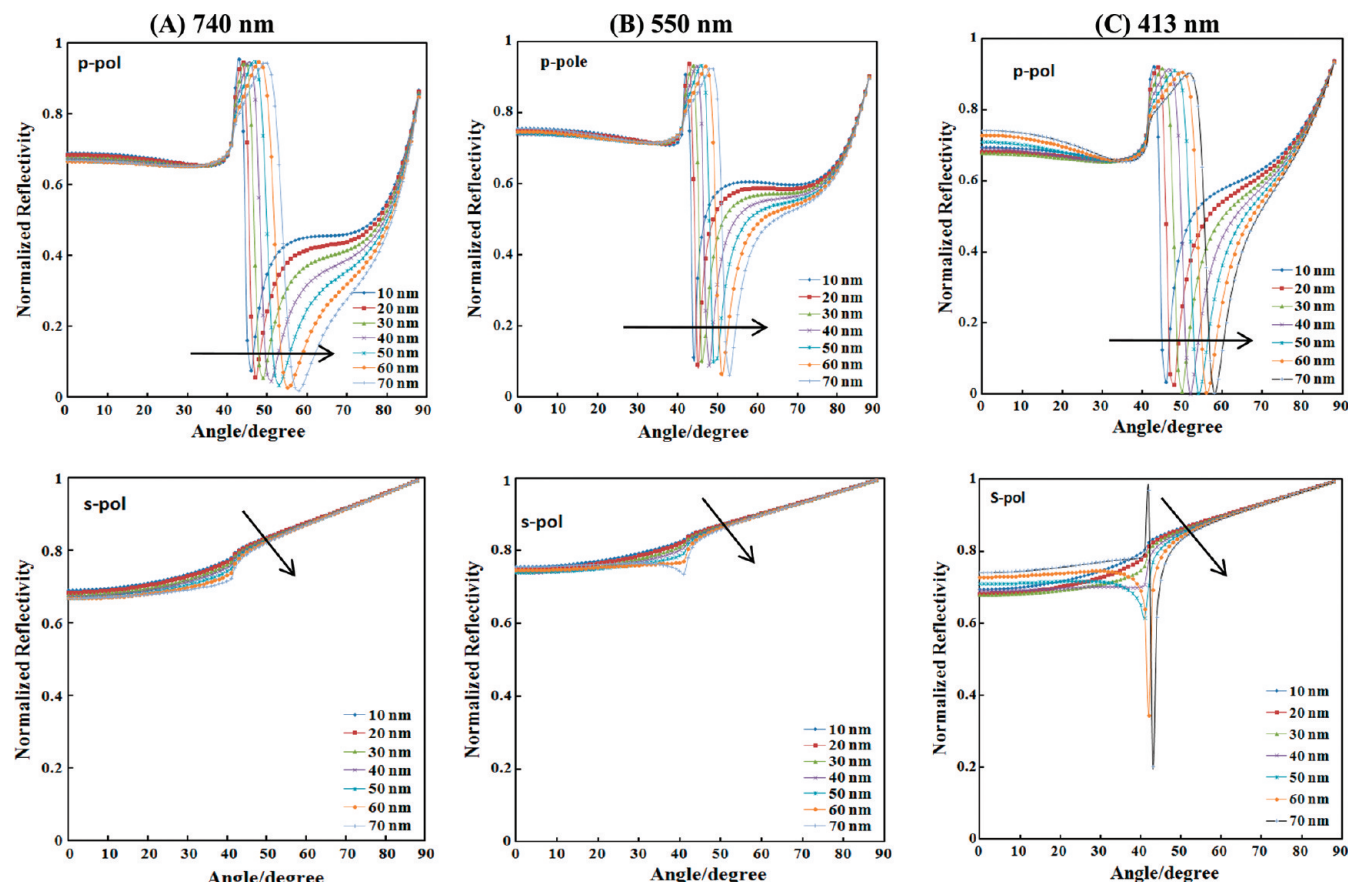


Figure 4. Five-phase Fresnel reflectivity curves for *p*-(top) and *s*-(bottom) polarized light at (A) 740 nm, (B) 550 nm, and (C) 413 nm for indium (20 nm) and SiO_x (20 nm), and PVA polymer coating thicknesses ranging from 10 to 70 nm.

70 nm are shown in the top and bottom of Figure 2, respectively. These calculations were employed to predict the interactions of *p*- and *s*-polarized light of different wavelengths with different thicknesses of indium thin films. The reflectivity values for different thicknesses have subsequently been normalized to compare the angle of minimum reflectivity. Reflectivity minimum is an indication of the efficiency of the surface plasmon generation in a metal film. At this angle of minimum reflectivity, dipoles couple to the surface plasmons and start to radiate at this particular angle. Further, coupled luminescence emission increases as the reflectivity decreases. Therefore, normalized reflectivity values can be qualitatively used to assess the thickness of the thin metal films in surface plasmon coupled fluorescence spectroscopy. As shown at the top of Figure 2, the angle of minimum reflectivity for *p*-polarized light for different thicknesses of indium thin films is approximately constant at 44° , and it has a minimum for 20 nm. Further, it is also observed that there is no change in the angle of minimum reflectivity for *p*-polarized radiation from the UV to the near IR. At the bottom of Figure 2, we can see that the reflectivity value of the *s*-polarized light decreases with increased thickness. From these calculations, we observed that the range of coupling of *p*-polarized light is much longer than the coupling of *s*-polarized light: from 207 to 840 nm (see Figures 1 and 2 in the Supporting Information). From these calculations, the ideal thickness for indium thin films was concluded to be about 20 nm.

In SPCS measurements, metallic thin films on glass slides are typically coated by SiO_x as a protective over coating. To optimize the thickness of the SiO_x layer, four phase (glass/metal/ SiO_x /air)

Fresnel reflectivity calculations were undertaken as shown in Figure 3. It is observed that the angle of minimum reflectivity increases with increasing SiO_x thickness. It is also observed that on decreasing the wavelength, the range of the angles of minimum reflectivity increases along with an increase in the area of minimum reflectivity. Figure 3D shows that a 20 nm SiO_x layer coated on a 20 nm indium thin film is predicted optimal for SPCF applications.

Finally, five-phase (glass/metal/ SiO_x /polymer/air) Fresnel reflectivity calculations for *p*-polarized and *s*-polarized light at 740, 550, and 413 nm were undertaken for different thicknesses of PVA layers (Figure 4), where the PVA coatings were used to locate the fluorophores close to the metal. The angle of minimum reflectivity for *p*-polarized light changes from 44° to 60° with an increasing thicknesses of the PVA. Reflectivity values for *s*-polarized light are found to increase on coating thin layers of the PVA films. It is also observed that for shorter wavelengths (413 nm), a sharp dip in reflectivity appears for *s*-polarized light. This suggests that a waveguide mode is present after the inclusion of a 40 nm thick layer of polymer. The absorption spectrum of glass coated with 20 nm In, 20 nm SiO_x , and 20 nm PVA are shown in Figure 3 of the Supporting Information. The plasmonic band of indium blue-shifted on protecting by SiO_x and PVA.

Figure 5 shows the experimental SPCF emission from selected fluorophores (pyridine-2, sodium fluorescein, and tinopal-CBS) and overlapped calculated Fresnel reflectivity curves corresponding to the wavelength of the emission peak of the fluorophores. Five-phase Fresnel reflectivity curves showing *p*- and *s*-polarized

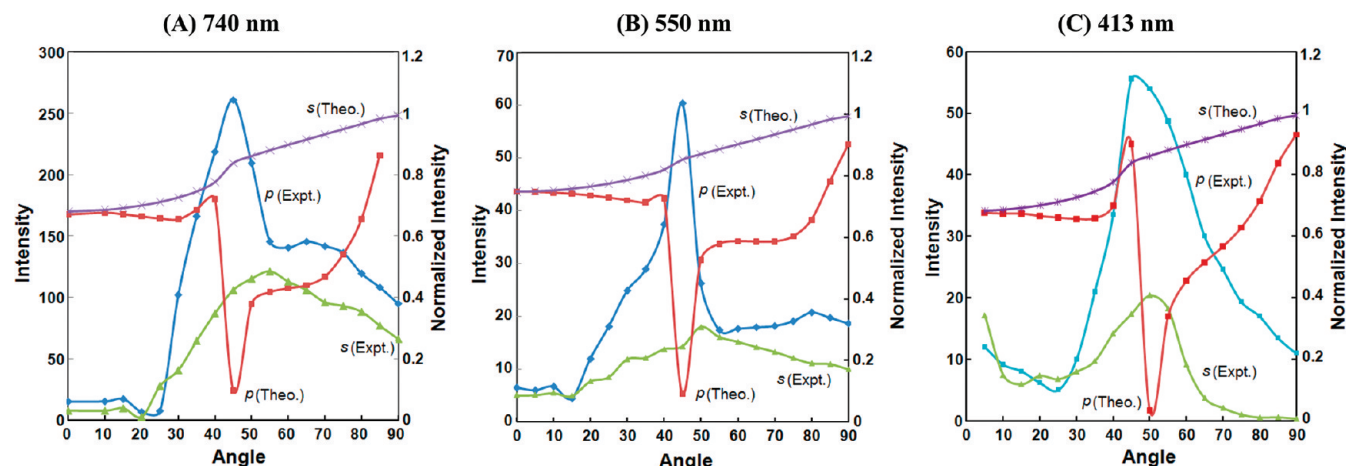


Figure 5. SPCF from indium substrates for (A) pyridine-2, (B) sodium fluorescein, and (C) tinopal-CBS. Five-phase Fresnel reflectivity curves showing *p*- and *s*-polarized light for ~ 20 nm indium substrates with ~ 20 nm SiO_2 and ~ 20 nm PVA over layers. Experimental *p*- and *s*-polarized emission collected at 413 nm for tinopal, 550 nm for sodium fluorescein, and 740 nm for pyridine-2.

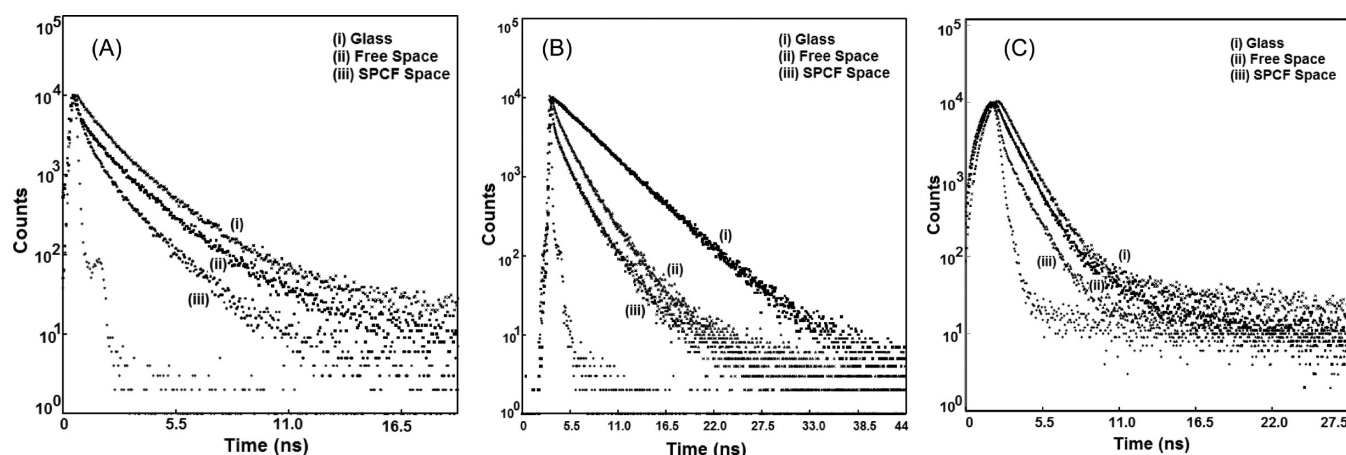


Figure 6. Decay curves of (A) pyridine-2, (B) sodium fluorescein, and (C) tinopal from (i) glass slides and In, SiO_2 , and PVA coated glass slides in both (ii) free space and (iii) SPCF space at $\lambda_{\text{ex}} = 445$ nm.

Table 2. Intensity Decay Parameters of NATA Doped in PVA and Coated on 20 nm Indium + 20 nm SiO_2 ($\lambda_{\text{ex}} = 282$ nm)^a

sample	τ_1 (ns)	τ_2 (ns)	τ_3 (ns)	α_1	α_2	α_3	$\langle \tau \rangle$	$\bar{\tau}$	χ^2
glass slide	2.56	0.56	5.25	47	5	48	4.35	3.75	0.990
free space	1.70	0.15	4.98	44	23	33	3.19	2.97	1.144
SPCF space	1.06	0.15	3.82	32	33	34	3.16	1.68	1.209

^a $\langle \tau \rangle$ is the amplitude weighted decay time. $\bar{\tau}$ is the mean decay time.

light for ~ 20 nm indium substrates with ~ 20 nm SiO_2 and ~ 20 nm PVA over layers are also shown. Experimentally, *p*- and *s*-polarized emissions were collected at 413 nm for tinopal, 550 nm for sodium fluorescein, and 740 nm for pyridine-2. It is interesting that significant agreement is observed between the experimental data and the theoretical predictions. Figure 5A shows a normalized *p*- and *s*-polarized fluorescence intensity from $10 \mu\text{M}$ pyridine-2 in PVA films deposited onto indium thin films. The SPCF emission from pyridine-2 coated indium thin films is measured at angles of 0 – 90° , and the free space emission

is measured at 120° . Fresnel reflectivity curves of light at 740 nm for the 20 nm indium thin films and an overlayer of 20 nm SiO_x and nearly 20 nm PVA are also shown. The fluorescence emission intensity at 740 nm is the highest at a 44° angle, where the reflectivity is minimum due to the coupling of the fluorescence emission to surface plasmons in indium thin films, suggesting the close agreement between theoretical and experimental data. The free space emission intensity was similar to that of the SPCF intensity measured at 44° . Fluorophore emission was only observed when the emission polarizer was in the *p*-orientation, meaning parallel to the plane of observation. The fluorescence signal was over 2.5-fold less for an *s*-oriented polarizer. The high *p*-polarization of the signal strongly suggests surface plasmon mediated emission and not free space emission.

In earlier studies, it was found that the spontaneous emission of fluorescent species close to metals were modulated, and a distance dependent radiative and/or nonradiative decay channel was observed.^{12,37} Therefore, we have undertaken time-domain fluorescence measurements for all three fluorophores in both free and SPCF space. The analyzed overlapped decay curves of pyridine-2, sodium fluorescein, and tinopal from a glass slide

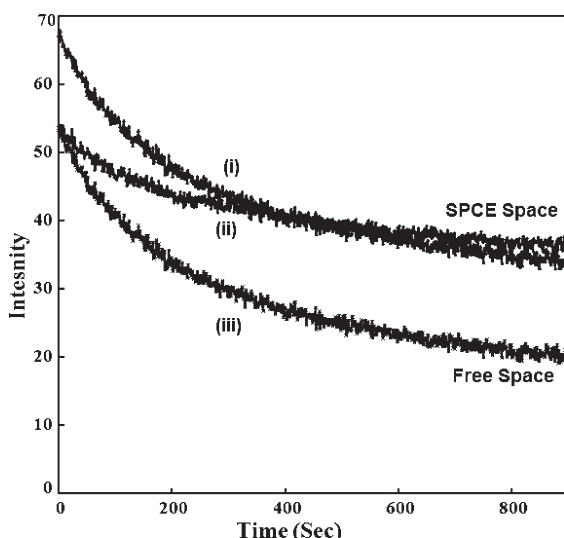


Figure 7. Intensity vs time (photostability) of sodium fluorescein in (i) SPCF space and (iii) in free space for an In (20 nm) + SiO_x (20 nm) + PVA (20 nm) coated glass slide at $\lambda_{\text{ex}} = 445$ nm. (ii) Shows the intensity decay of sodium fluorescein fluorescence, where the initial steady-state intensity at $T = 0$ has been adjusted to the same free space value using excitation neutral density filters.

and In, SiO₂, and PVA coated glass slides in both free space and in SPCF space excited by $\lambda_{\text{ex}} = 445$ nm are shown in Figure 6. The analyzed decay data are given in Table 2. Both the amplitude-weighted decay time and average decay time in the free space emission and SPCF were found to decrease with respect to a glass slide, i.e., in the free space condition. This dramatic decrease in decay times is similar to those observed in MEF studies.¹¹ Further, in order to understand the decrease in decay time of fluorophores in free and SPCF space, we also measured the photostability of sodium fluorescein sample. The fluorescence intensity variation of sodium fluorescein with time is shown in Figure 7. Not unexpectedly, it is observed that the photostability of the sodium fluorescein increases in the surface plasmon coupled emission (SPCE) space, as compared to the isotropic free space condition.

To understand the range of distances over which fluorophores couple with surface plasmons, z-axis evanescent field intensity values were estimated by further using Fresnel calculations for different wavelengths, as shown in Figure 8A. This distance is indicative of the penetration depth of the surface plasmon evanescent field into the sample and of the near field excitation volume. It is found that the evanescent wave generated by longer wavelengths (740 nm) can penetrate up to 300 nm in comparison to shorter wavelengths (413 nm). It is also observed that with respect to silver (a widely used substrate in SPCF), evanescent waves can penetrate approximately twice the distance (Figure 8B). These results suggest that the optical properties of indium for SPR and SPCF are favorable in the UV region and will be thus probably useful for intrinsic protein fluorescence studies.

In this regard, here we have additionally undertaken both steady-state and time-resolved protein fluorescence measurements. Interestingly for the indium films, not only is intrinsic protein SPCF detected but also metal enhanced fluorescence is also observed in the free space. Figure 9A shows overlapped five-phase Fresnel reflectivity curves for *p*- and *s*-polarized light at 350 nm, with indium (20 nm) + SiO₂ (20 nm) + PVA polymer

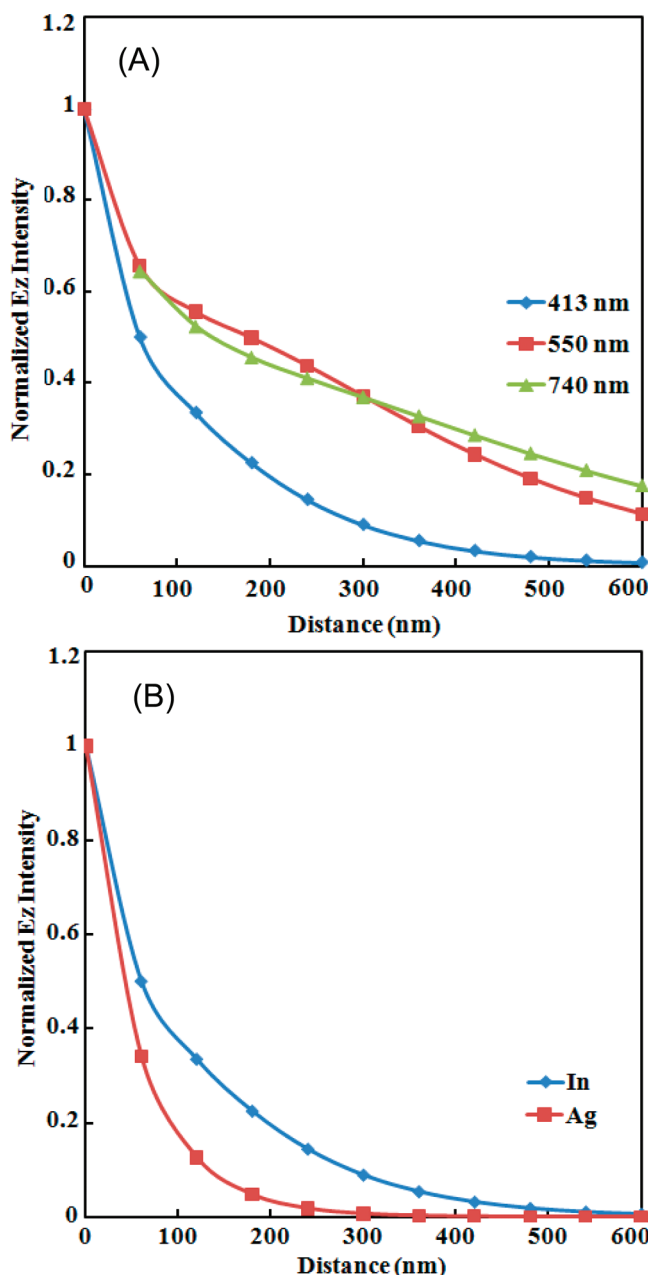


Figure 8. (A) Relative z-axis evanescent wave intensity (intensity from surface) for different wavelengths and (B) its comparison with a thin silver substrate (20 nm) at 413 nm.

(20 nm) on a glass plate along with the observed fluorescence spectra of NATA in SPCF space. Similar to the other fluorescent dyes, emission from the SPCF space was only observed when the emission polarizer was in the *p*-orientation, i.e., parallel to the plane of observation, and the intensity of this signal was again about 20 times higher than that in the *s*-polarized plane. This again suggests the coupling of NATA fluorescence to indium surface plasmons at the prism interface. Figure 9B shows the free space metal-enhanced fluorescence spectra of NATA in PVA on a glass slide and on the indium film, with an excitation wavelength of $\lambda_{\text{ex}} = 280$ nm at a concentration of 10^{-3} M. About a 3.5-fold enhancement is observed in NATA emission in the free space. Further, time-resolved measurements were also undertaken and

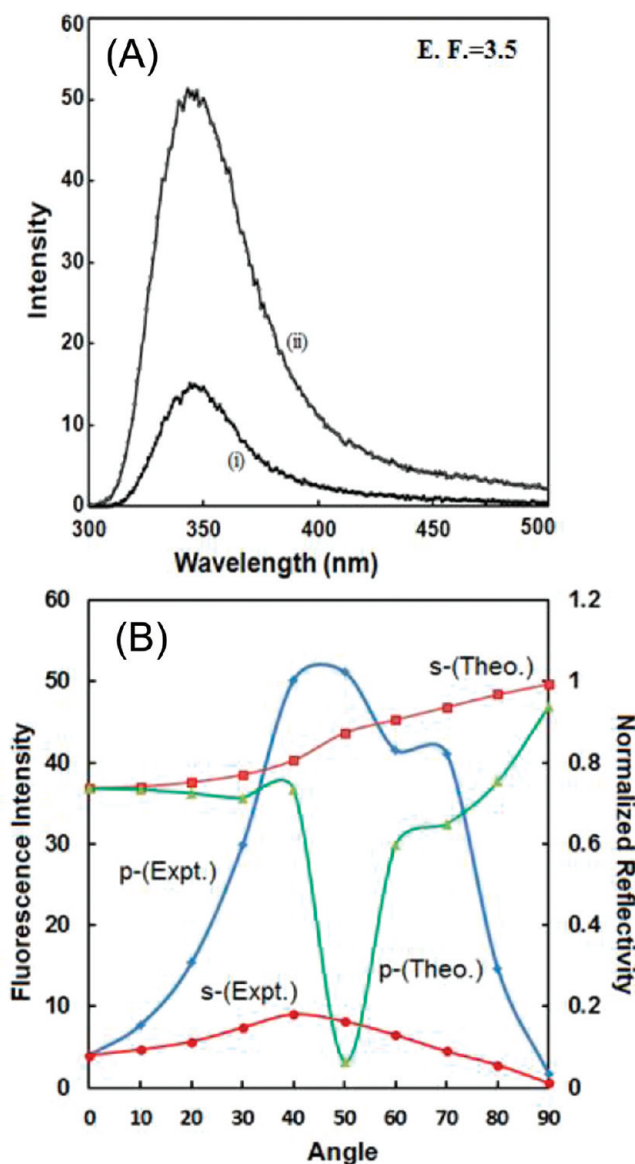


Figure 9. (A) Free space metal-enhanced fluorescence spectra of NATA in PVA on (i) a glass slide and on (ii) In (20 nm) + SiO_x (20 nm) + PVA (25 nm), at an excitation wavelength of $\lambda_{ex} = 280$ nm [concentration 10^{-3} M]. (B) Overlapped five-phase Fresnel reflectivity curves for *p*- and *s*-polarized light at 350 nm, In (20 nm) + SiO_x (20 nm) + PVA polymer (25 nm) on a glass plate along with the observed fluorescence spectra of NATA in SPCF space.

the data summarized in Table 2. The overlapped decay curves of NATA from glass and on indium films are additionally shown in Figure 4 of the Supporting Information. Again, it is found that both the amplitude-weighted decay time and average decay time in the free space emission and for SPCF were found to decrease with respect to a glass slide, i.e., a control sample where no surface plasmon phenomena are present. The observation of ultraviolet SPCF and MEF with indium suggests numerous potential applications in biochemistry, biotechnology, and medical testing. UV fluorophores are routinely used to label proteins and membranes, and our findings suggest that both enhanced and directional protein fluorescence are measurable, i.e., for the label-less detection of biomolecules.

4.0. CONCLUSIONS

Indium thin film experimental results are shown to be in complete agreement with reflectivity curves that have theoretically been predicted using multiphase Fresnel calculations. Reflectivity curves predict broad wavelength transmission, suggesting applicability to analytical sensing in the ultraviolet to NIR spectral regions. These predict that the excitation evanescent field can penetrate to a greater distance than other metal thin films, making the indium thin films an excellent choice of metal to be used in SPCF applications. Indium thin films generate highly polarized and directional emission in the SPCF space. Fresnel calculations also predict that light at 207 to 850 nm can effectively couple to 20 nm indium thin films at a fixed six degree wide observation angle, located between 44° to 50° from the normal of the surface. Indium thin films have the potential to be a single assay platform in SPCF and SPR over a broad wavelength range. Since the SPCF from indium thin films can be observed at a fixed angle for such a wide wavelength range, no adjustment in the angle of detection optics would be needed. This is especially attractive for the incorporation of metal thin films into existing fluorescence technologies and/or instruments, and for the development of a generic fluorometer that is based on SPCF. Of particular interest in this work, is that indium thin films can enhance intrinsic protein fluorescence, which is likely to find multifarious applications for the label-less detection of biomolecules.

■ ASSOCIATED CONTENT

S Supporting Information. Additional results of theoretical and experimental characterization of indium films and optical parameters of indium are presented in four figures and one table. This material is available free of charge via the Internet at <http://pubs.acs.org>.

■ AUTHOR INFORMATION

Corresponding Author

*Phone: +1-410-576-5720. E-mail: geddes@umbc.edu.

■ ACKNOWLEDGMENT

We acknowledge the Institute of Fluorescence (IoF) and the Department of Chemistry and Biochemistry at the University of Maryland Baltimore County, USA for financial support.

■ ABBREVIATIONS

- MEF: metal enhanced fluorescence
- SPCE: surface plasmon coupled emission
- SPCL: surface plasmon coupled luminescence
- SPCF: surface plasmon coupled fluorescence
- SPFS: surface plasmon fluorescence spectroscopy
- NATA: *N*-acetyl-tryptophan-amide

■ REFERENCES

- (1) Peterson, W.; Halter, M.; Tona, A.; Bhadriraju, K.; Plant, A. L. *BMC Cell Biol.* **2009**, *10*, 16.
- (2) *Handbook of Surface Plasmon*; Schaafert, R. B. M., Tudos, A. J. Eds.; RSC Publications: London, 2008.
- (3) Ong, B. H.; Yuan, X. C.; Tjin, S. C. *Fiber Integr. Opt.* **2007**, *26*, 229.
- (4) Margarida, M.; Vareiro, L. M.; Liu, J.; Knoll, W.; Zak, K.; Williams, D.; Toby, A.; Jenkins, A. *Anal. Chem.* **2005**, *77*, 2426–2431.

- (5) Rothenhausler, B.; Knoll, W. *Nature* **1988**, *332*, 615.
(6) Giebel, K.-F.; Bechinger, C.; Herminghaus, S.; Riedel, M.; Leiderer, P.; Weiland, U.; Bastmeyer, M. *Biophys. J.* **1999**, *76*, 509–516.
(7) Knoll, W. *Annu. Rev. Phys. Chem.* **1998**, *49*, 569–638.
(8) Liedberg, B.; Nylander, C.; Lundstrom, I. *Biosens. Bioelectron.* **1995**, *10*, R1.
(9) Szabo, A.; Stolz, L.; Granzow, R. *Curr. Opin. Struct. Biol.* **1995**, *5*, 699.
(10) Tully, J. C. *Annu. Rev. Phys. Chem.* **2000**, *51*, 153–78.
(11) *Metal-Enhanced Fluorescence*; Geddes, C. D., Ed.; Wiley International: New York, 2010.
(12) Radiative Decay Engineering. In *Topics in Fluorescence Spectroscopy*; Geddes, C. D., Lakowicz, J. R., Eds.; Springer: New York, 2004; Vol. 8.
(13) Knoll, W. *Coll. Surf. A* **2000**, *171*, 115–130.
(14) Gryczynski, I.; Malicka, J.; Gryczynski, Z.; Nowaczyk, K.; Lakowicz, J. R. *Anal. Chem.* **2004**, *76*, 4076–4081.
(15) Kwon, S. H.; Hong, B. J.; Park, H. Y.; Knoll, W.; Park, J. W. *J. Colloid Interface Sci.* **2007**, *308*, 325–331.
(16) Liu, J.; Tiefenauer, L.; Tian, S.; Nielsen, P. E.; Knoll, W. *Anal. Chem.* **2006**, *78*, 470–476.
(17) Tawa, K.; Yao, D.; Knoll, W. *Biosens. Bioelectron.* **2005**, *21*, 322–329.
(18) Aslan, K.; Previte, M. J.; Zhang, Y.; Geddes, C. D. *J. Immunol. Methods* **2008**, *331*, 103–113.
(19) Matveeva, E.; Gryczynski, Z.; Gryczynski, I.; Lakowicz, J. R. *J. Immunol. Methods* **2004**, *286*, 133–140.
(20) Aslan, K.; Malyn, S. N.; Geddes, C. D. *J. Immunol. Methods* **2007**, *323*, 55–64.
(21) Geddes, C. D.; Gryczynski, I.; Malicka, J.; Gryczynski, Z.; Lakowicz, J. R. *J. Fluoresc.* **2004**, *14*, 119–123.
(22) Ford, G. W.; Weber, W. H. *Phys. Rep.* **1984**, *113*, 195–287.
(23) Morawitz, H.; Philpott, M. R. *Phys. Rev. B* **1974**, *10*, 4863–4868.
(24) Dostálek, J.; Knoll, W. *Biointerphases* **2008**, *3*, 12–22.
(25) Homola, J. *Chem. Rev.* **2008**, *108*, 462–493.
(26) Aslan, K.; Geddes, C. D. *Anal. Chem.* **2009**, *81*, 6913.
(27) Aslan, K.; Previte, M. J.; Zhang, Y.; Geddes, C. D. *Anal. Chem.* **2008**, *80*, 7304.
(28) Gryczynski, I.; Malicka, J.; Gryczynski, Z.; Nowaczyk, K.; Lakowicz, J. R. *Anal. Chem.* **2004**, *76*, 4076.
(29) Liebermann, T.; Knoll, W. *Colloids Surf., A* **2000**, *171*, 115–130.
(30) Smith, D. S.; Kostov, Y.; Rao, G.; Gryczynski, I.; Malicka, J.; Gryczynski, Z.; Lakowicz, J. R. *J. Fluoresc.* **2005**, *15*, 895.
(31) Aslan, K.; Zhang, Y.; Geddes, C. D. *Anal. Chem.* **2009**, *81*, 3801.
(32) Gryczynski, I.; Malicka, J.; Nowaczyk, K.; Gryczynski, Z.; Lakowicz, J. R. *J. Phys. Chem. B* **2004**, *108*, 12073.
(33) Previte, M. J. R.; Zhang, Y. X.; Aslan, K.; Geddes, C. D. *Appl. Phys. Lett.* **2007**, *91*, 10.
(34) Zhang, Y.; Padhyay, A.; Sevilleja, J.; Guerrabt, R. L.; Geddes, C. D. *J. Phys. Chem. C* **2010**, *114*, 7575–7581.
(35) Geddes, C. D.; Gryczynski, I.; Malicka, J.; Gryczynski, Z.; Lakowicz, J. R. *J. Fluoresc.* **2004**, *14*, 119–123.
(36) Dragan, A. I.; Geddes, C. D. *J. Appl. Phys.* **2010**, *108*, 094701.
(37) Barnes, W. L. *J. Mod. Phys.* **1998**, *45*, 661–699.